Advancements in EMI simulators for radiated immunity and emissions testing

A dual polarization broadband gigahertz field simulator for measuring immunity and emissions of electronic equipment meets many criteria for advanced testing programs.

ANDREW S. PODGORSKI
ASR Technologies
Ottawa, Canada

JOZEF BARAN
AST Computer
Irvine, CA

The expansion of wireless communication and the growth of high power microwave (HPM) technology is shifting the interest of the EMC community to the requirements for broadband, continuous wave and pulse testing at gigahertz frequencies. One result is a new concept for a dual polarization broadband gigahertz field (BGF) simulator for the measurement of immunity and emissions of electronic equipment. The dual polarization BGF simulator allows fully automated immunity and emissions testing of electronic and electrical equipment, in both polarizations, in accordance with the existing European (IEC 61000-4-3) and North American (ANSI C63-4) standards. The simulator can be installed into either semi-anechoic chambers or anechoic chambers. In contrast to existing methods, the simulator does not require change or rotation of test antennas, and when conducting immunity testing, there is no need to install absorbing material on the floor. The full automation of immunity and emission measurements in the simulator, and a ten-fold reduction of the testing time, result in substantially lower costs for the user.

BROADBAND GIGAHERTZ FIELD (BGF) SIMULATOR

The simulator was initially conceived as a single polarization simulator, either horizontal or vertical, capable of operating in the frequency range from DC to at least 40 GHz. Later, the simulator was developed as a dual polarization simulator with two versions implemented—anechoic and semi-anechoic chamber design. The anechoic chamber design can be used for testing different sized ground-free structures, such as mobile phones or aircraft in flight, while the semi-anechoic chamber design can be used to test structures that require a ground plane, such as systems using power outlets.

This article addresses the dual polarization simulator, installed into a semi-anechoic chamber and used simultaneously for immunity and emission measurements in both polarizations. A cross-section of the simulator is shown in Figure 1.

The simulator technology is based on a hybrid concept that utilizes two testing techniques:

- Transmission lines for testing at frequencies below 80 MHz
- Large horn antennas at frequencies above 80 MHz.

In Figure 1, one vertical polarization horn antenna and two horizontal polarization horns are attached to the walls of a semi-anechoic chamber. The antennas positions are fixed. The septum of each

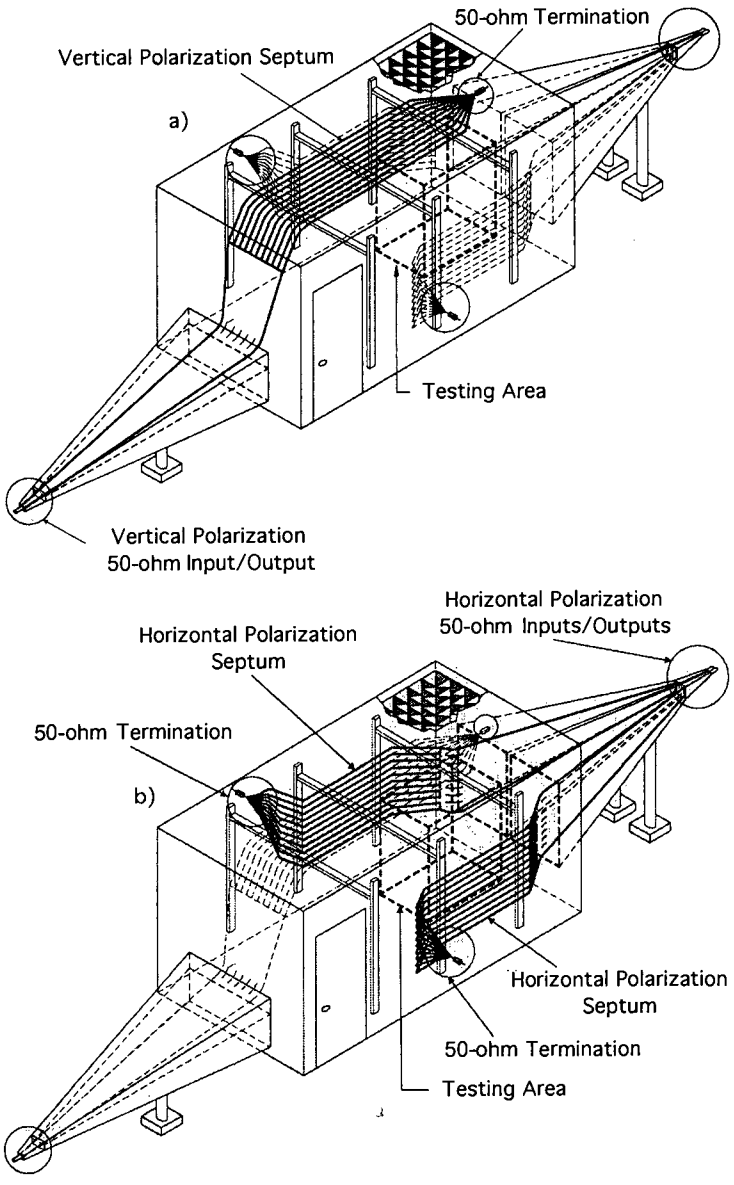

Figure 1. Cross-section view of dual polarization BGF simulator: (a) vertical polarization, and (b) horizontal polarization.

of three horns is extended in the form of wire transmission lines along the walls and ceiling of the semi-anechoic chamber. To avoid reflection at frequencies above 80 MHz, the wire transmission lines are hidden between the cones of the semi-anechoic chamber absorbers. Each wire transmission line is terminated with a 50-ohm resistor that, depending upon requirements, can be located either inside or outside the chamber.

The first dual polarization BGF simulator, for simultaneous testing in vertical and horizontal polarization of immunity[1] and emission[2], was built in 1995. The simulator was fully automated, permitting not only the instantaneous change from immunity to emission measurement, but also an immediate change from vertical to horizontal polarization. The BGF simulator was built into a semi-anechoic chamber having internal shielded room dimensions of 6.78 m x 3.7 m and 2.77 m high. The resultant operational volume is 3.8 m x 2.3 m and 2.1 m high.

In this BGF simulator, the dimensions of 1.5 m width and 1.0 m height, positioned 80 cm above the ground that are required for emissions tests (ANSI Std. C63.4) were maintained, and the recommended 30-cm spacing from the test area to the anechoic material is retained.

For immunity testing in accordance with IEC 61000-4-3, the required electric field uniformity of 0 to -6 dB in a test area of 150 x 150 cm was preserved. Moreover, the operational frequency range of 1 GHz imposed by both ANSI C63.4 and IEC 61000-4-3 was extended up to 5 GHz to accommodate the requirements. However, one should keep in mind that, even considering that present computer clock frequencies are already reaching 500 MHz and still increasing, the upper frequency limit of the simulator can easily be expanded to 40 GHz to allow the 10th harmonic testing of faster, future systems.

IMMUNITY TESTING

Currently, the immunity measurements are conducted in accordance with IEC 61000-4-3. The standard requires that measurements be taken in the frequency range of 80 to 1000 MHz, at the electric field uniformity of 0 to -6 dB, in the testing area of 150 cm x 150 cm. Such electric field uniformity needs to be maintained in 12 out of 16 field points that are equally spaced in the prescribed testing area.

Until now, the immunity measurements were usually done using biconical and log-periodic antennas in semi-anechoic chambers. However, to achieve the electric field uniformity in the specified frequency range, the metallic floor of the chamber must be covered with absorbing material.

Presently, only the BGF simulator is known to achieve the IEC 61000-4-3 requirements of field uniformity of 0 to -6 dB

- in both polarizations (vertical and horizontal)
- in the frequency range 27 MHz to 5000 MHz

- in the testing area of 150 cm x 150 cm (allowing testing of objects as high as 150 cm)
- with no need for changing the test antennas or installing the absorbing material on the floor.

An example of BGF simulator field uniformity measured at frequencies 27, 80, 303.82 and 1000 MHz, using a 16-point method per IEC 61000-4-3 is illustrated in Figure 2. The test results indicate that in the frequency range from 27 to 1000 MHz, the electric field uniformity at 12 points is always maintained. Moreover, for the frequencies lower than 200 MHz (27 to 80 MHz), the electric field uniformity is maintained for all 16 points. This is attributed to the use of TEM-mode septum design in the BGF which ensures exceptional uniformity of the generated electromagnetic field.

The use of the dual polarization simulator also ensures that the requirement imposed by IEC 61000-4-3 for the electric field intensity of 10 V/m can be achieved by using two 25-W power amplifiers. Since there is no need to use absorbing material on the floor of the BGF, the testing area of 150 cm x 150 cm can be located only 10 cm above the ground. The testing of floor-standing equipment then becomes possible. As a result, the one test setup can be used for both immunity and emission testing.

Based on the performance of the simulator, it was approved for immunity testing in accordance with IEC 61000-4-3 by NEMKO, the European Authorized Body of Norway on Feb. 13, 1996.

EMISSIONS TESTING

Presently, the emissions measurements are conducted in accordance with ANSI C63.4-1992. Although this standard requires that emissions be measured in the frequency range 30 to 1000 MHz, and that the tested object be placed in the testing area of 100 cm (height) x 150 cm (width), located 80 cm above the ground, it is common practice to measure the emission up to the 10th harmonic of the emission source (computer clock). Until now, the emissions measurements were most often done using biconical, log-periodic and horn antennas at Open Area Test Sites (OATS), or they were done in an alternative site such as a semi-anechoic chamber or GTEM cell. ANSI C63.4-1992 requires that all measurements done in an alternative site be within 4 dB of the measurements taken at an OATS.

Currently, the emissions measurements at OATS and in the semi-anechoic chambers require that the tested object be horizontally rotated (incremental 360°), so that the most radiating side of the tested object is found. In addition, the receiving antennas are raised from a height of 1 m to 4 m above the ground, so that the maximum emission resulting from the summary of direct and ground reflected signals is determined. Unlike testing in the BGF, the results of emissions measurements done at an OATS are affected by the ground loss of the site and by the environmental noise level. In the case of the semi-anechoic chamber, the need to raise the receiving antenna to a height of 4 m imposes a requirement that the test chamber height be at least 6 m—a very expensive proposition.

In the BGF simulator (as in the semi-anechoic chambers and on OATS), the incremental 360° horizontal rotation of the tested object permits location of the most radiating side of the tested object. However, in the simulator, the maximum total of direct and ground-reflected emission signals is found by raising and lowering the tested object from its standard height of 80 cm above the ground, rather than by the up-and-down movement of the receiving antennas. Moreover, the use of the transmission line concept in the simulator assures that only a 30-cm movement of the tested object from its standard height (80 cm) is required. This small movement does not affect the tested object radiation pattern, nor does it affect the radiated signal strength. The small 30-cm movement of the tested object (versus a 300-cm antenna movement on an OATS or in semi-anechoic chambers), allows much faster measurement of the maximum emission signal. Since there is no need for a change of antennas or antenna polarizations, this small movement of the tested object results in reduced testing time by an order of magnitude.

The computer-conducted, comparative emission measurements at an OATS and in the dual polarization simulator spanned two years. The results indicated a very good correlation of the emission data for laptop, desktop and server computers measured in the simulator and on OATS. Figure 3 illustrates the differences in the amplitude of the emissions signal with respect to the reverse limits of the OATS and the simulator where the reverse limits are defined as a maximum acceptable voltage at the spectrum analyzer input which corresponds to the E-field emission limits specified by ANSI. Figure 3 indicates that, with vertical polarization, the emission test results in BGF versus OATS do not exceed 3.0 dB, and with horizontal polarization, the deviation of the emissions test results in the BGF versus the OATS do not exceed 3.5 dB. The difference in the readings between the BGF and the OATS never exceed those imposed by ANSI C63.4, Para 5.4.6.1, or 4 dB.

Based on the proven performance of the simulator, it was accepted as an alternative test site for emission testing by the U.S. Federal Communication Commission (FCC) on October 16, 1998.

CONCLUSIONS

A BGF simulator can be installed in either semi- or fully-anechoic chambers. When the BGF is installed in a semi-anechoic chamber, the semi-anechoic chamber height required is less than half that required in a semi-anechoic chamber used in standard

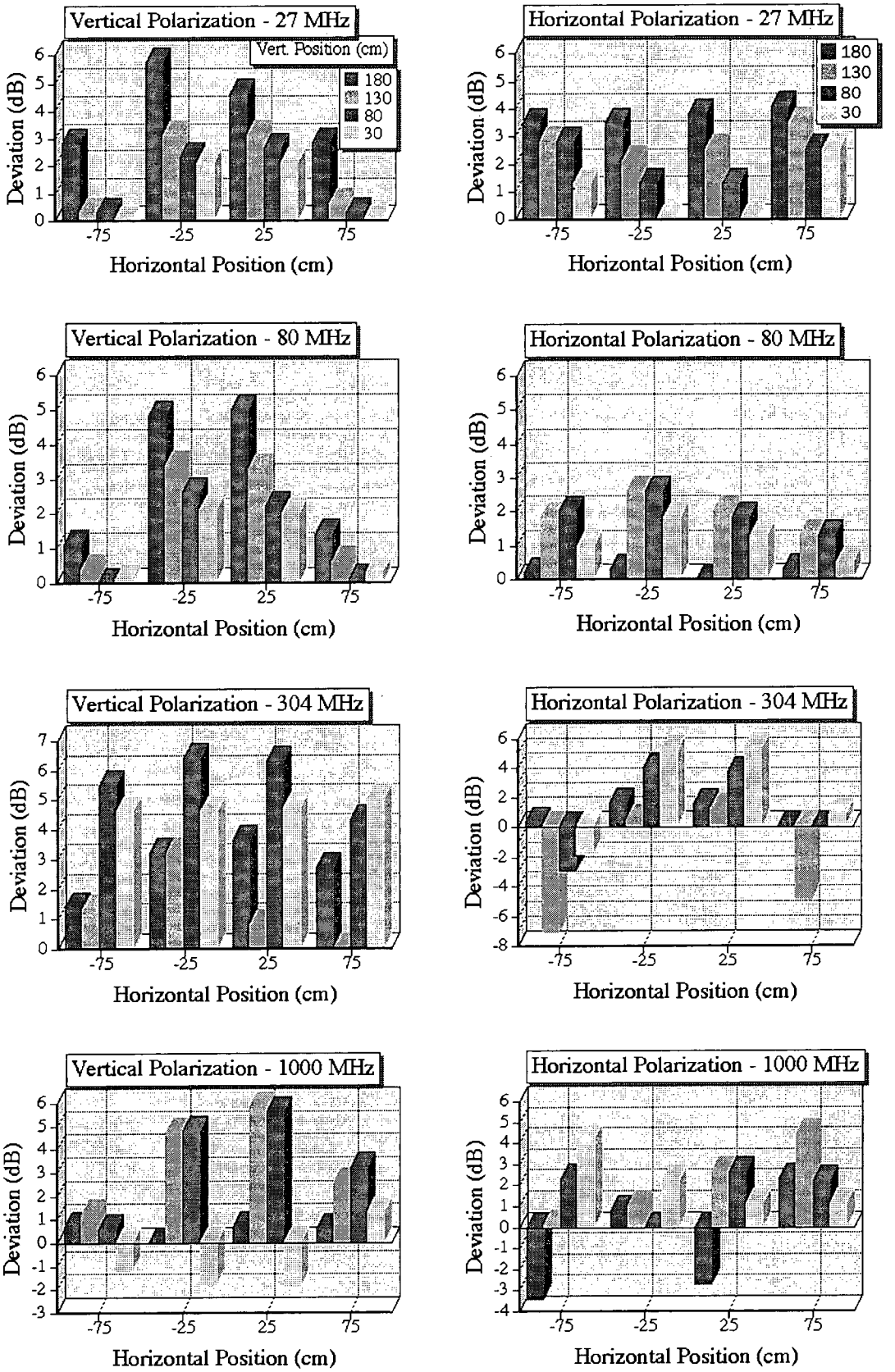

Figure 2. Deviation of the electric field from the nominal value of 3 V/m (0 dB) measured in a 1.5-m x 1.5-m grid, per IEC Std. 61000-4-3.

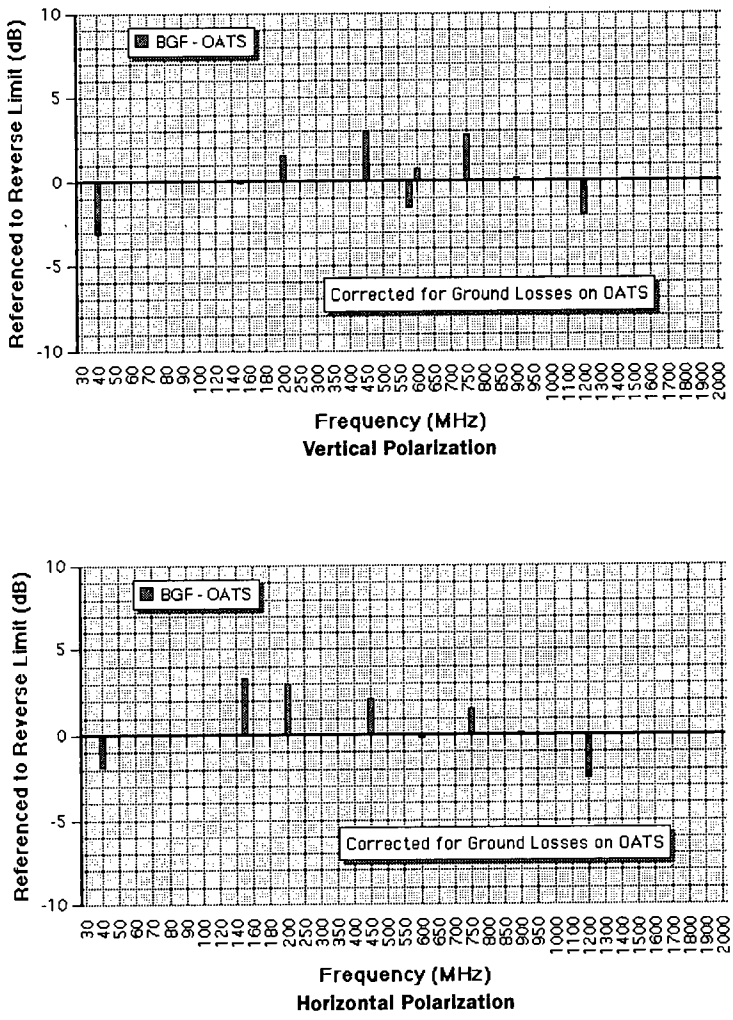

Figure 3. Computer No. 1–Differences in amplitude of the emission signal with respect to the reverse limits of OATS and BGF (max. ± 4 dB as per ANSI C63.4).

emission measurements. Currently, the immunity and emissions measurements can be taken in both horizontal and vertical polarizations, in the frequency range from a few kHz to an extended frequency range of at least 40 GHz, with no need for vertically rotating the test object or changing the position or type of test antenna. The currently imposed requirement by IEC 61000-4-3 for a testing area of 150 x 150 cm can be modified to accommodate testing of different sized objects (mobile phones or aircraft) at field strengths as high as 50 kV/m.

For immunity testing, the imposed standard field uniformity of 0 to -6 dB is achieved in the testing area of 150 x 150 cm, and the field intensity of 10 V/m required by the IEC 61000-4-3 is achieved in the BGF, at low cost, with two 25-W amplifiers. The immunity testing is done without violation of environmental ambient field requirements. Since no absorbing material is required on the floor, the same test setup can be used for both immunity and emissions testing.

For emissions testing, the transmission line concept in the BGF ensures that only a 30-cm movement of the tested object from its standard height (80 cm) is required, allowing much faster determination of measured maximum emission signal. The emissions testing is free from ambient interference and ground losses.

The ability to use the BGF simulator as a new installation or as a modification to existing installations, easy access to the testing area, full automation of measurements, and therefore, ten-fold reduction of the testing time, are key factors which endorse use of the BGF.

REFERENCES

1. A. S. Podgorski and J. Baran, "New Concept of Emission and Susceptibility Testing," Proceedings of the 1997 IEEE International Symposium on EMC, August 18-22, 1997, Austin, Texas, pp. 497-499.
2. A. S. Podgorski and J. Baran, "Radiated Emission Measurements Conducted in the AST Semi-Anechoic Chamber Dual Polarization Broadband Gigahertz Field Simulator and Their Verification with the Measurements Done on the Open Area Test Site," Proceedings of the 1998 IEEE International Symposium on EMC, Denver, Colorado, August 24-28, 1998, pp. 854-859.

ANDREW S. PODGORSKI *received his Ph.D degree in electrical engineering from the University of Waterloo, Ontario, Canada in 1980. Currently, he is President of ASR Technologies, a research and development company conducting research in the area of broadband electromagnetics. A prolific writer and the holder of many patents related to broadband electromagnetics, Dr. Podgorski has served on many international and inter-governmental panels of experts representing Canada. In 1992, he was elected to the Board of Directors of the Electromagnetic Compatibility (EMC) Society of the IEEE and he is currently the Chair of the Technical Activities Committee. He is a Life Member of the IEEE EMC Society and he was a "Distinguished Lecturer" for the Society. (613) 737-2026. a.podgorski@ieee.org.*

JOZEF BARAN *received a Masters' degree in electrical engineering from Wroclaw Technical University in 1970 and joined AST Research Inc. in 1987. Currently, Mr. Baran is a senior principal EMC engineer and department manager for the EMC Engineering, Product Safety, and Reliability Engineering Departments at AST. Mr. Baran is involved in EMI control in printed circuit board design and he is a NARTE-certified EMC engineer as well as an active member of the IEEE EMC Society. (949) 587-9723.*

ground planes/traces decreases, the possibility of sparks and arcing in the inter-line spacings and the chances of breakdown in the board substrates increase. The main concerns are arcing between the circuit board traces and breakdown in the insulation substrates that could be detrimental to components and circuit boards used in electronic equipment circuit cards.

In the analyses and discussions that follow, it will be assumed that, in pursuit of new trends in circuit board technology, the line spacing and the inter-layer substrate thickness have decreased such that the threat of inter-trace arcing and inter-substrate breakdown exists. Since using circuit boards crowded with smaller line spacings will find extensive application in the foreseeable future, the ultimate goal is to provide these circuit boards with protection from lightning-induced transients. That is, the objective is to protect the circuit board and the circuit card components from failure and permanent damage, to immunize the functional operations of the circuit cards to upset, and to safeguard the MTBF of the circuit board from degradation.

CIRCUIT BOARD TRACE-INDUCED VOLTAGE THEORY

In general, evaluation of the lightning-induced transient voltages at the circuit board interface traces in avionics equipment may require application of complicated techniques used in coupled mode theory using distributed circuit parameters for traces acting as portions of strip transmission lines. Such is the case when lightning transients, such as short duration Waveform 2 and 10-MHz damped sinusoidal Waveform 3 voltages, are the sources of induced currents in cable wiring with lengths comparable to the wavelength of the frequency content of the transient waveform. However, for induced lightning transients of longer duration such as Waveform 3, 1-MHz damped sinusoidal, or Waveforms 4 and 5 transient pulses, and under conditions of sufficiently small cable wiring lengths and circuit dimensions, the well-established elementary lumped circuit theory can be applied. In order to enhance and demonstrate the existence of large lightning-induced voltages between the traces, the circuit board trace-induced voltage theory is developed for application to typical cable wiring and trace impedance terminations which are specifically selected to confirm the agreement of the experimental results with developed theory based on the well-known lumped circuit theory. For the sake of analysis simplicity, it is assumed that the impedances Z_i and Z_o imposed by lightning are resistive, as are found in most of the circuit card designs (Figure 9).

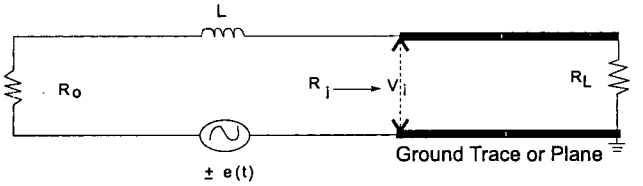

Figure 9. Single interface trace-induced lightning voltage theory.

SINGLE TRACE COMMON-MODE LIGHTNING-INDUCED VOLTAGES

The lightning-induced current flowing into a trace in a single wiring loop is then related to the lightning-induced voltage e(t), the loop self-inductance L, and the input and output impedances R_i and R_o by the well-known lumped circuit equation as follows:

$$e(t) = (R_i + R_o)I(t) + L\frac{d\,I(t)}{dt} \qquad (1)$$

In the case of large terminating input and output impedances $R_i + R_o$, the loop self-inductance termination has insignificant effect on the loop lightning-induced current. In this case, the trace lightning-induced voltage at the trace input with terminating impedance R_i becomes

$$V_i(t) = I(t)R_i = \frac{R_i\, e(t)}{R_i + R_o} \qquad (2)$$

Then for the input loads $R_i << R_o$, the total terminating impedances $R_i + R_o \cong R_o$, and

$$V_i(t) = \frac{R_i\, e(t)}{R_i + R_o} \cong \frac{R_i}{R_o} e(t) \qquad (3)$$

which indicates that the trace voltages are much smaller than the loop lightning induced voltage e(t).

For $R_i >> R_o$, the ratio $\dfrac{R_i}{R_o + R_i} \cong \dfrac{R_i}{R_i} = 1$ and

$$V_i(t) = \frac{R_i\, e(t)}{R_i + R_o} = e(t) \qquad (4)$$

proving that the trace voltage may become as large as the loop lightning-induced voltage. For the special case of $R_i = R_0$,

$$V_i(t) = \frac{R}{R_i + R_o} e(t) = \frac{e(t)}{2} \qquad (5)$$

LIGHTNING-INDUCED VOLTAGES BETWEEN TWO NEIGHBORING TRACES

The dependence of common-mode induced voltages on the loop termination impedances are well understood by considering Equations 2 through 4. The equations for the trace-induced common-mode voltage $e_a(t)$ and $e_b(t)$, and the induced currents $I_a(t)$ and $I_b(t)$ flowing into Traces A and B (Figure 10) due to lightning, can be expressed as

$$e_a(t) = L_a \frac{dI_a(t)}{dt} + I_a(t)R_{ia} + I_a(t)R_{oa} \pm M_{ab} \frac{dI_b}{dt} \quad (6)$$

$$e_b(t) = L_b \frac{dI_b(t)}{dt} + I_b(t)R_{ib} + I_b(t)R_{ob} \pm M_{ab} \frac{dI_a}{dt} \quad (7)$$

where

L_a and L_b = Self-inductance of the cable wiring loops connected to Traces A and B respectively

R_{ia} and R_{oa} = Input and output impedances at Trace A

R_{ib} and R_{ob} = Input and output impedances at Trace B

M_{ab} = Mutual inductance of the wiring loops terminating on Traces A and B

Note that the mutual capacitance between the loops that may have some effect on the potential difference between the traces is neglected. This assumption can be proved valid because of the long duration of the induced lightning pulses involved in this analysis. Also, a no-load termination between the adjacent traces has been assumed for further simplification in analysis and for further enhancement in the inter-trace potential difference.

In general, $e_a(t)$ and $e_b(t)$ may vary for wiring loops of different dimensions and for different categories of lightning environments. However, when the two cable interconnect wiring loops terminating on Traces A and B are in the same lightning environments and have equal loop dimensions, $e_a(t)$ and $e_b(t)$ can be considered equal ($e_a(t) = e_b(t)$).

As in the case of single-trace, common-mode induced voltages, for large values of the total loop terminating input and output impedances, both self- and mutual-inductance terms have an insignificant effect in limiting the induced lightning currents. The loops $I_a(t)$ and $I_b(t)$ are considered to depend primarily on the input and output trace impedances, yielding the following loop voltage equations:

$$e_a(t) = I_a(t)(R_{ia} + R_{oa}) \quad (8)$$

$$e_b(t) = I_b(t)(R_{ib} + R_{ob}) \quad (9)$$

For $R_{ia} \ll R_{oa}$, the sum

$R_{ia} + R_{oa} \cong R_{oa}$, and for $R_{ib} \gg R_{ob}$, the ratio $\frac{R_{ib}}{R_{ib} + R_{ob}} \cong 1$

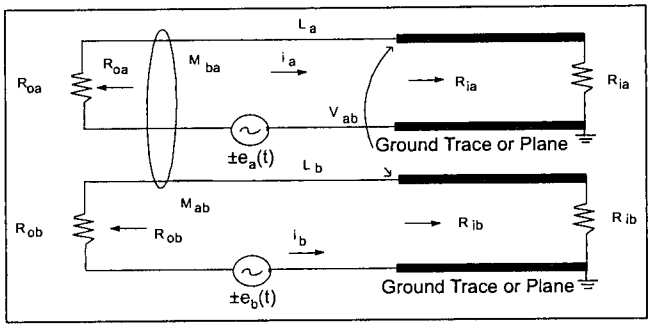

Figure 10. Two-trace induced lightning voltage theory.

Then the trace voltages become equal to

$$V_a(t) = I_a(t)\, R_{ia} = \frac{e_a(t)\, R_{ia}}{R_{ia} + R_{oa}} \cong e_a(t) \frac{R_{ia}}{R_{oa}} \quad (10)$$

$$V_b(t) = I_b(t)\, R_{ib} = \frac{e_b(t)\, R_{ib}}{R_{ib} + R_{ob}} \cong e_b(t) \quad (11)$$

The trace potential is then obtained as

$$V_{ba} = e_b(t) - e_a \frac{R_{ia}}{R_{oa}} \quad (12)$$

Assuming no common impedance within the loads at the end of the lines, both theoretical calculation and experimental results indicate that the inter-trace mutual capacitance has no effect on the R_{ia}/R_{oa} ratio.

In the case where $e_b(t) = e_a(t)$, the potential difference equation yields

$$V_{ba} = e_a(t)\left[1 - \frac{R_{ia}}{R_{oa}}\right] \quad (13)$$

Equation (13) indicates that when inequality relations $R_{ia} \ll R_{oa}$ and $R_{ib} \gg R_{ob}$ hold, the potential difference between the neighboring traces may approach the wiring loop lightning-induced voltages.

EXPERIMENTAL VERIFICATION

In order to verify the potential differences which appear between circuit card traces, and to confirm the validity of Equations (4) and (13) derived in the theory, an experiment was performed using the wiring configuration and load termination found in a typical avionics cable. The 12-foot long avionics cable consisted of 13 wires terminated in typical circuit card input and output loads, such as protective diodes, 12-kohm resistors simulating ARINC 429 inputs, 10-kohm discrete inputs, small resistors and shorts simulating other input and output trace impedances (Figure 11).

The circuit card input and output impedances in each wiring loop were chosen so that at any typical trace, such as Trace A, the total loop impedance $R_{ia} + R_{oa}$ was larger than 12 kohm in order to simulate a typical avionics equipment. The large total impedance made the loop currents small, and therefore, the self- and mutual-inductance terms in Equations (9) and (10) are negligible as compared to the $i_a (R_{ia} + R_{oa})$ or $i_b (R_{ib} + R_{ob})$ terms. The list of input and output trace impedances is provided in Table 1.

The cable bundle was routed through a ferrite core coupling transformer with the cable wiring loops forming the inductively coupled turns of the transformer secondary. The wiring loop lightning-induced voltages were simulated by injecting pulses from a damped sinusoidal pulse generator connected to the single turn primary of a ferrite core transformer.

The pulse generator output was adjusted until an open-circuit peak voltage of 800 V at a secondary turn, small calibration loop terminal was recorded. In order to avoid the severe noise variations in the damped sinusoidal first peak, the 800-V peak voltage was referenced to the second peak. Nevertheless, a 2- to 5-percent variation in the peak voltage was noticed as the simulated lightning-induced voltages between the trace and ground, or between the traces, was measured.

With the trace input and output impedances acting as the transformer secondary loads, the damped sinusoidal pulses were injected into the cable wiring bundle. Trace potential to ground V_{ag}, V_{bg}, ... V_{mg} and the potential difference between traces V_{ab}, V_{ac}, ... V_{am}, V_{bc}, V_{bd}, ... V_{bm}, etc. was measured at the input wiring terminal using a storage oscilloscope with a differential input. The measured data for all the input traces (wire terminals) a, b, c, ... m, is provided in Table 2.

The effect of inter-trace potential differences causing arc and sparkover between traces was confirmed by connecting the traces on a circuit board to the cable bundle terminal pins, a, b, c, d, and f. The arcing and sparkover was initiated when the potential difference was increased and the electric field level for breaking down the inter-trace was reached. The effects of mutual induction between the cable bundle wiring was also investigated by increasing the current in one of the cable wires. The increased current in the wire, terminated on Trace *A*, was achieved by reducing the output impedance at Trace A to zero. The result of the experiment indicated that in a cable with 13 tightly bundled high-impedance wiring loops, the low impedance wire at Trace A reduced the trace voltage and inter-trace potential by approximately 4 dB. Further reductions of 6 dB and 12 dB in inter-trace potential differences were obtained by increasing the number of low impedance wires to 2 and 4 respectively. Based on these experimental results, no further significant reductions in potential difference could be reached, even when the number of low impedance wiring loops increased above 4.

Low-impedance wiring loops in the cable bundle are effective in inter-trace potential reduction only if they are in parallel with other cable loops in the same bundle. Any loop which terminates on circuit card traces through the same connector, but is not part of the main cable wiring bundle, may remain unaffected by the cable low impedance loops. This finding was supported by experiments and showed that the potential difference between Trace n and the main cable wiring traces will remain independent of the number of low impedance loops in the wiring (Figure 11).

SUMMARY

State-of-the-art circuit card operational function design has been concerned with common-mode voltages most often limited to 30 Vdc and differential voltages varying between -15 to +15 V. Lightning-induced voltages generated by the lightning environment result in common-mode

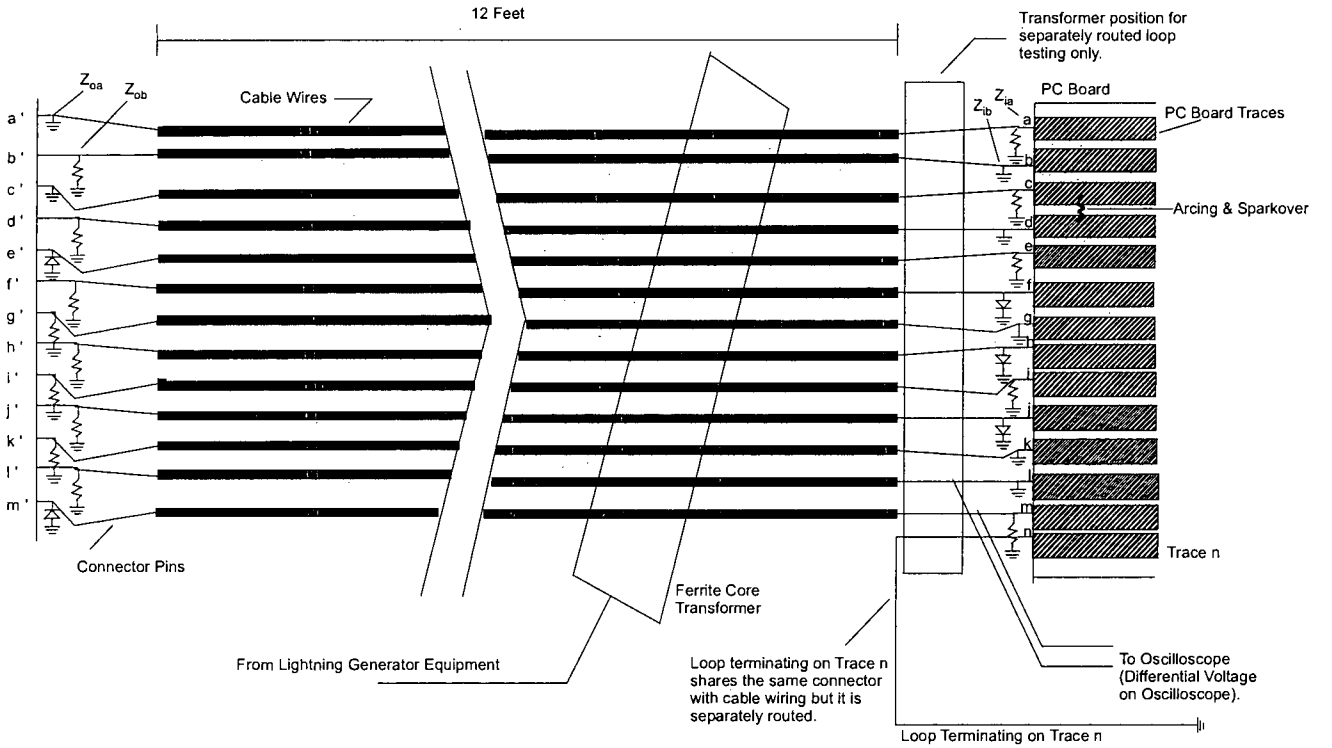

Figure 11. Twelve-foot cable bundle with 13 parallel cables and one cable not in parallel connected to terminating loads and PC board traces through wires simulating connector pins.

Trace Terminal	a	b	c	d	e	f	g
Input Impedance	12 kΩ	short	12 kΩ	short	12 kΩ	1N5646	short
Output Impedance	short	12 kΩ	short	12 kΩ	1N5646	12 kΩ	12 kΩ

Trace Terminal	h	i	j	k	l	m
Input Impedance	1N5646	10 kΩ	1N5646	short	short	12 kΩ
Output Impedance	10 kΩ	10 kΩ	12 kΩ + 1N5646	12 kΩ	12 kΩ	1N5646

Table 1. Input and output trace impedances.

Trace	a	b	c	d	e	f	g	h	i	j	k	l	m
P to Gnd V_{ag},... V_{mg}	800	0	800	0	800	44	0	46	<5	780	0	0	780
P to Trace V_{ab},... V_{am}		780	0	800	50	760	780	760	780	50	780	780	50
V_{bc},... V_{bm}			760	0	760	44	0	48	<5	780	0	0	760
V_{cd},... V_{cm}				800	46	780	800	760	800	45	800	800	45
V_{de},... V_{dm}					800	40	0	42	<5	780	0	0	780
V_{ef},... V_{em}						780	800	780	800	0	820	820	0
V_{fg},... V_{fm}							46	12	48	780	48	48	740
V_{gh},... V_{gm}								48	<5	760	0	0	780
V_{hi},... V_{hm}									42	780	40	760	760
V_{ij},... V_{im}										760	<5	0	780

Note: P = Potential

Table 2. Experimental data measurements.

voltages up to 1500 V peak which have often been suppressed to a maximum of 50 V peak using semiconductors, transistors, or varistors deployed as voltage clamping devices. Differential-mode voltages induced between the circuit card traces have been of little concern with respect to clamping, design safety, or component reliability evaluation.

This article proves, that as a result of new input and output impedances imposed on the circuit cards by the lightning protection devices and components in the lightning environment, the differential mode voltages which appear between the traces are significant and large enough that they should be clamped or their resulting electric field reduced. The results of the analysis indicate that inter-trace voltages can easily approach the magnitude of the loop voltages induced by the lightning. Since the wiring loop lightning-induced voltages in high lightning environments may reach 1500 V peak levels, carefully designed trace spacings and protective devices are required in order to prevent the adverse effects of sparkover between the circuit card traces as well as between the circuit card traces and the ground planes.

The accuracy of the theory has been proven by the experimental measurements provided herein. The evidence of the sparks appearing between the traces resulting from trace potential differences proves that protection of electronic components from lightning effects is important, as is protection of the circuit board itself.

REFERENCES

1. David Jennings, Balu Rudra, "Failure Mechanism Models for Conductive Filament Formations," *IEEE Transactions on Reliability*, Vol. 43, No. 3, September 1994, pp. 354-360.
2. Michael Pecht, Balu Rudra, "Assessing Time-To-Failure Due to Conductive Filament Formation in Multi-Layer Organic Laminates," *IEEE Transactions on Components, Packaging, and Manufacturing Techniques*, Part B, Vol. 17, No. 3, August 1994, pp. 269-276.
3. RTCA, "Environmental Conditions and Test Procedures for Airborne Equipment," DO-160C, *Radio Technical Commission for Aeronautics Specification*, Section 22, Change 2, June 19, 1992 and DO-160D, July 29, 1997.
4. FAA, "Protection of Aircraft Electrical/Electronic Systems Against the Indirect Effects of Lightning," *AC 20-136, FAA Advisory Circular*, March 5, 1990.
5. Fisher, Perala, and Plumer, "Lightning Protection of Aircraft," *Lightning Technology Inc.*, Pittsfield, MA, 1990.

ACKNOWLEDGMENTS

This work has been made possible thanks to the cooperation and support of Jim Law, Honeywell Defense Systems, and John Covell and Stuart Scott, Rockwell Collins, Inc. I would also like to thank Rockwell Collins, Inc., Cedar Rapids, Iowa for the funding and permission to publish this paper.

SADEGH M. VAKIL *attended the Technical University of Tehran and received the BSEE and MSEE degrees from the University of Missouri in 1958 and 1959 respectively. He joined Boeing Co. in Seattle, WA in June 1960 and was involved in research on electrical properties of soil and development of new techniques in measurement of filter insertion loss. From 1963 to 1969 he was employed by Lockheed Missiles and Space Division, Sunnyvale, California, where he worked on EMP/EMI analysis and testing. While at Lockheed, he attended the University of California at Berkeley, from which he received an MA degree in physics and completed the requirements to earn a Ph.D. in electrical engineering. In 1969 he joined the staff of Arya-Mehr University of Technology in Tehran, Iran and taught courses in engineering electromagnetics and physics. Since 1982, he has worked as a lightning/EMC specialist at Rockwell Corporation, Collins Avionics, in Cedar Rapids, Iowa. Mr. Vakil is a member of Tau Beta Pi and Eta Kappa Nu. (319) 295-8902.*